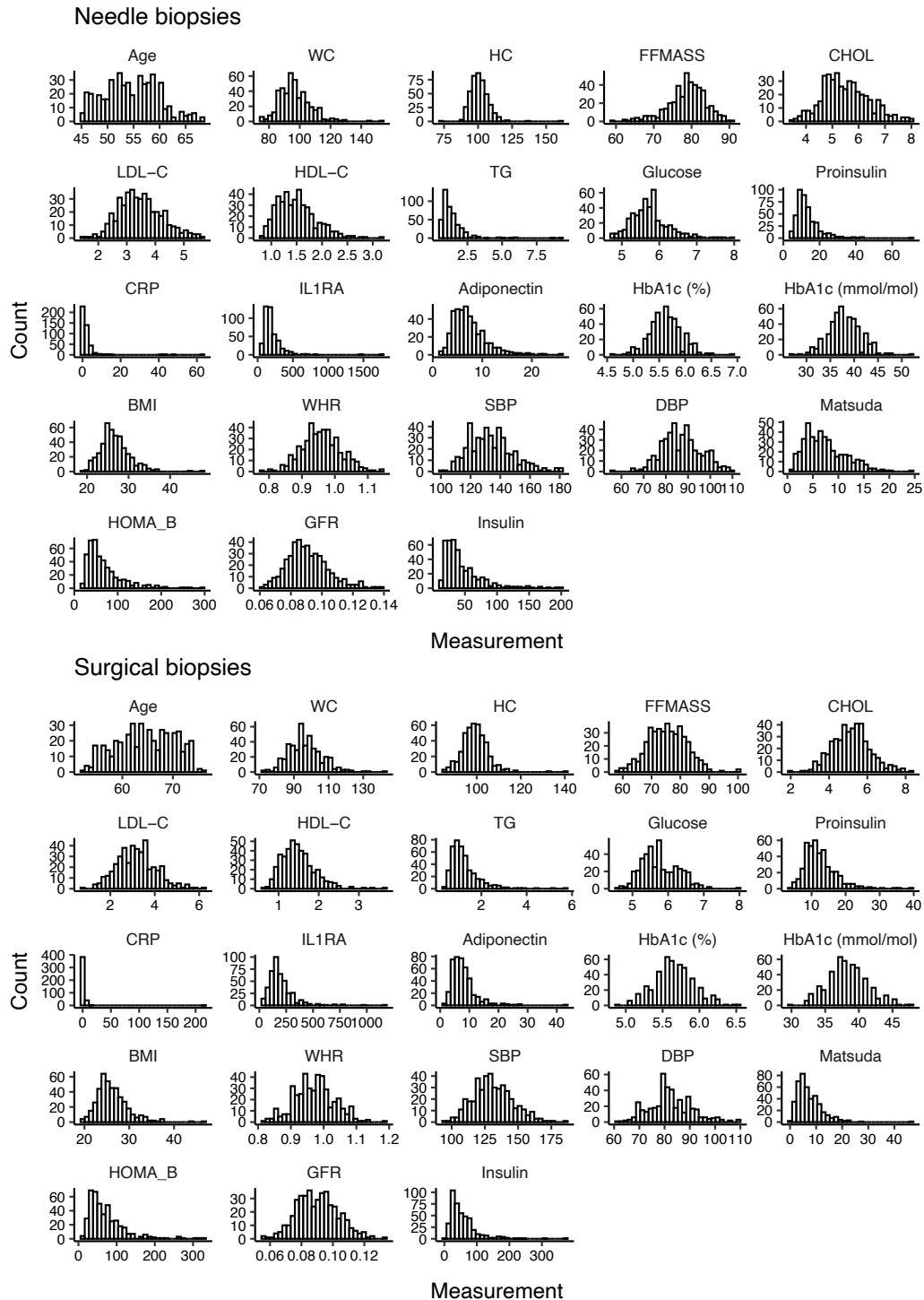
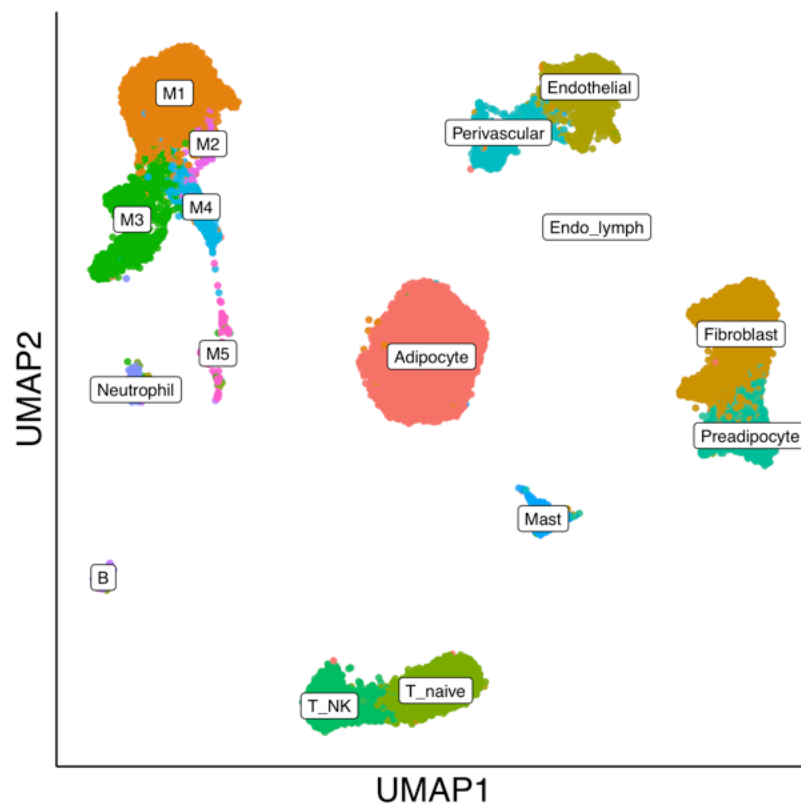


## Supplemental Figures



**Figure S1. Distribution of cardiometabolic trait measurements across individuals**  
 Histograms of 22 cardiometabolic trait measurements across all samples. The upper plots show needle biopsies ( $n = 434$ ), and the lower plots show surgical biopsies ( $n = 425$ ). The x-axes show trait values with units corresponding to Table S2. The y-axes show the counts of individuals in each bin.



**Figure S2. UMAP of snRNA-sequencing dataset (n = 16)**

UMAP of cell types from snRNA-seq dataset of 16 adipose tissue samples. Lymphatic endothelial cells were excluded from further analyses because they represent less than 1% of cells. M1-M5 are macrophage subgroups that were combined into one macrophage group for deconvolution.

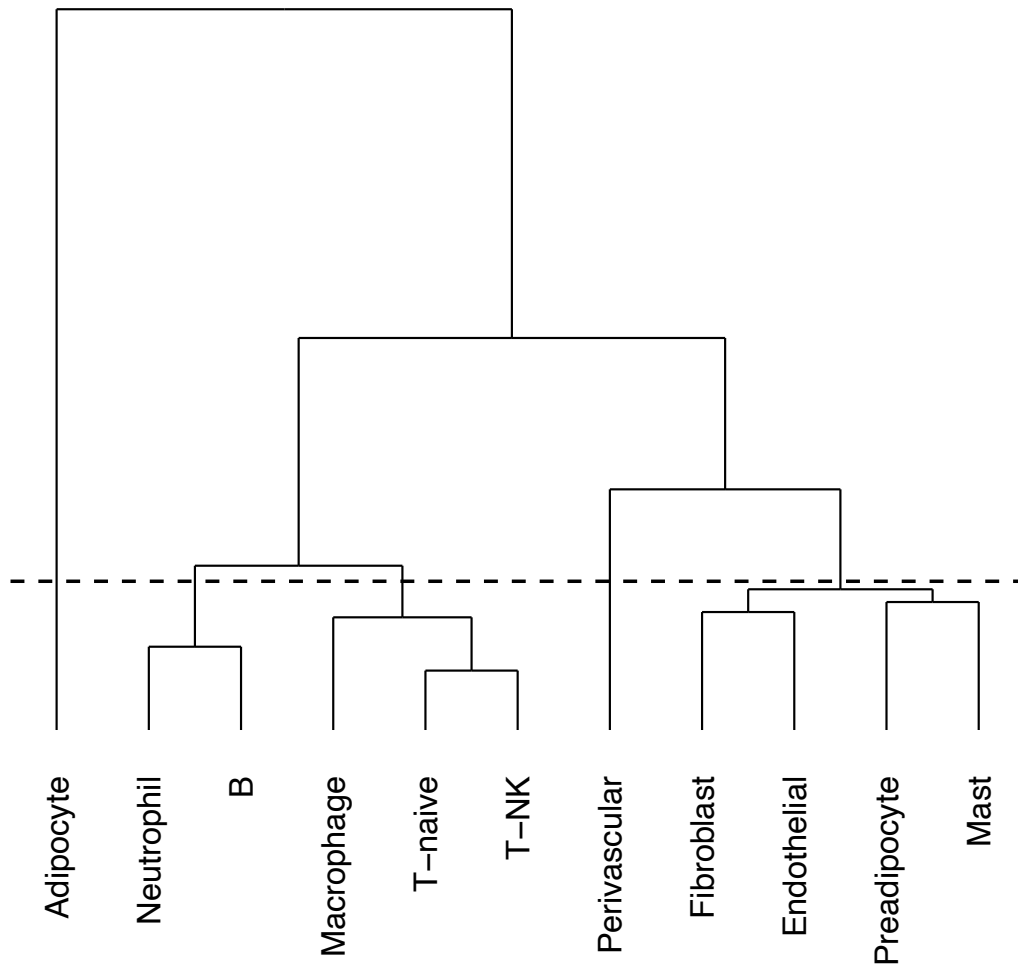


**Figure S3. Cell type clustering for SCDC tree-based deconvolution**

Clustering of cell types using Euclidian distance. The branches under the dotted line are clustered based on the first node for the SCDC tree-based deconvolution. The groups are: 1) Adipocyte; 2) Neutrophil and B; 3) Macrophages, T-naïve, and T-NK; 4) Perivascular; and 5) Fibroblast, Endothelial, Preadipocyte, and Mast.

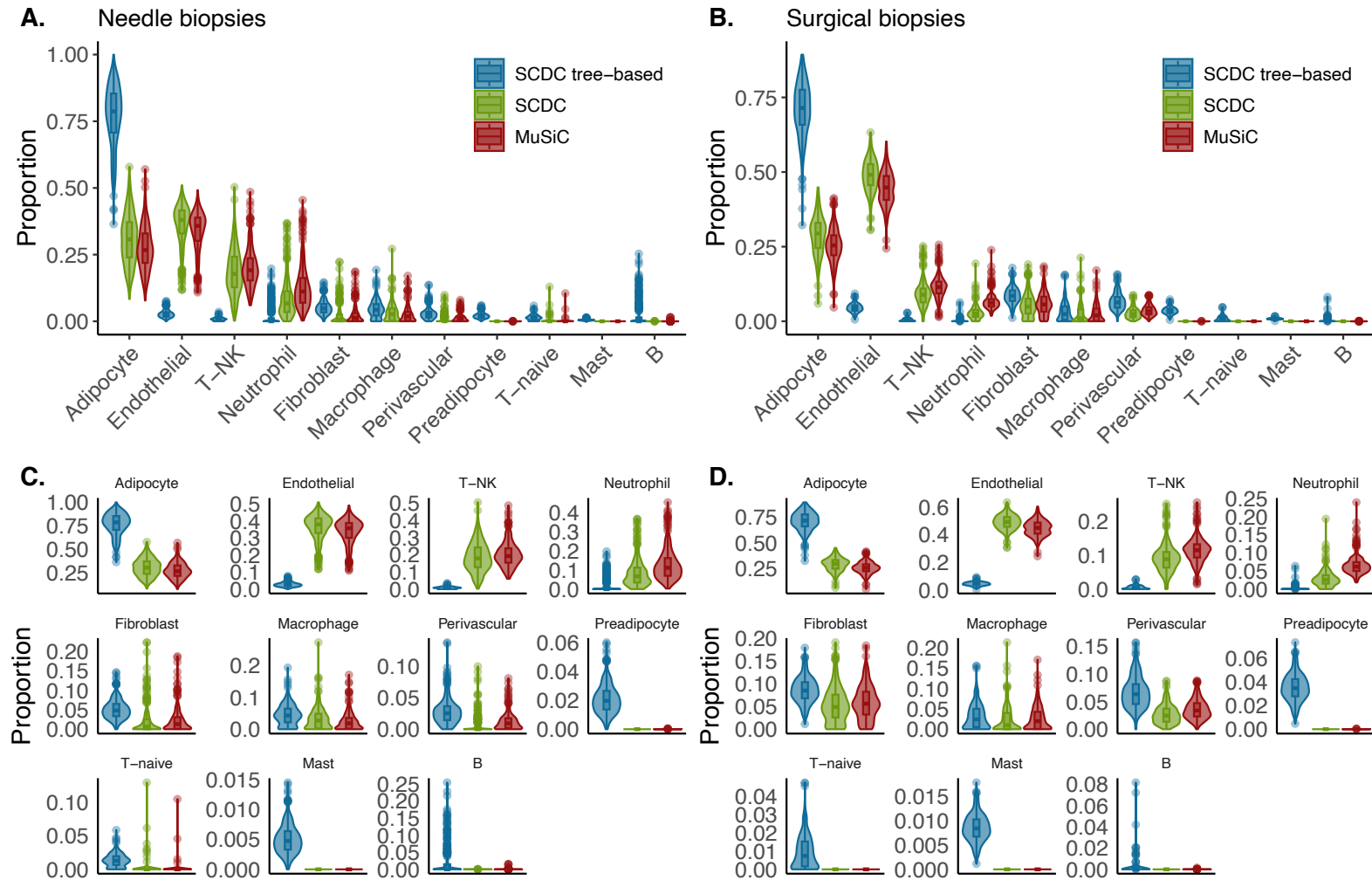


**Figure S4. Cell-type proportion estimates using different deconvolution strategies**

A. Violin plots of the cell-type proportion estimates across the needle biopsies (n = 434) using three deconvolution strategies: SCDC tree-based (blue), SCDC (green), and MuSiC (red). Boxplots within each violin plot show the median and interquartile range, and outliers are shown as dots.

- B. Violin plots of the cell-type proportion estimates across the surgical biopsies ( $n = 425$ ) using three deconvolution strategies as in A.
- C. Zoomed in violin plots of the cell-type proportions from A with a different plot for each cell type. The y-axes differ across plots.
- D. Zoomed in violin plots of the cell-type proportions from B with a different plot for each cell type. The y-axes differ across plots.

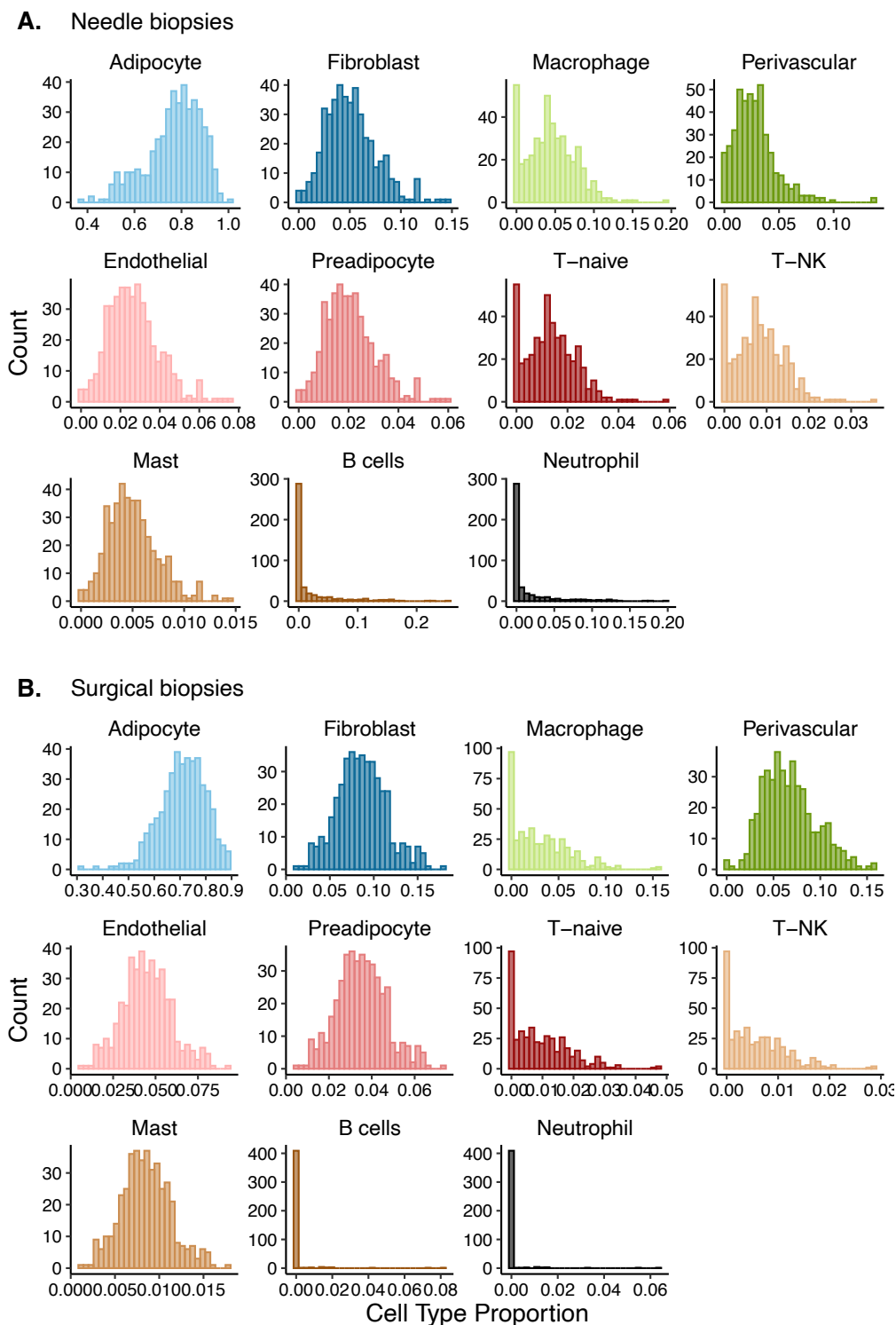


**Figure S5. Distributions of cell-type proportions across individuals**

- A. Histograms of cell-type proportions across needle biopsies (n = 434) using the SCDC tree-based deconvolution strategy. Each cell type has a different plot and a different color.
- B. Histogram of cell-type proportions across surgical biopsies (n = 425) as in A.

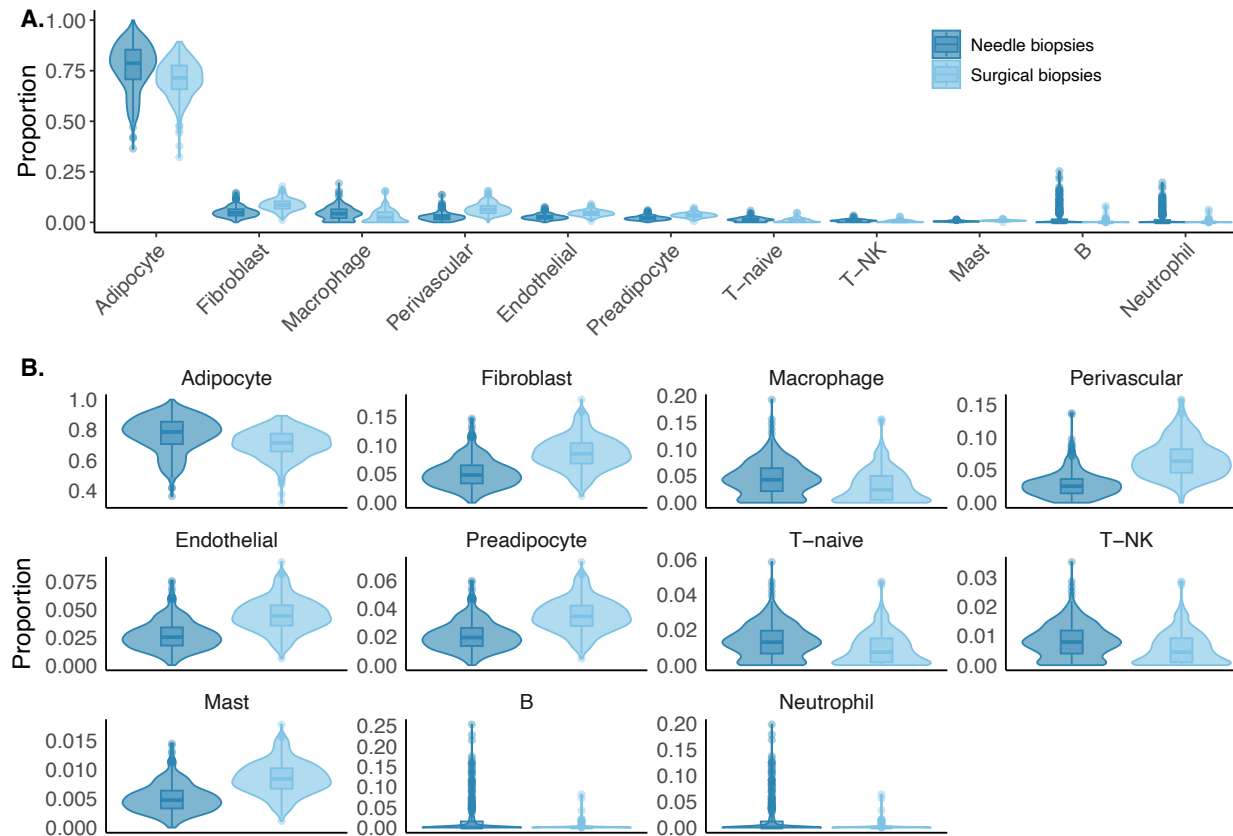


**Figure S6. Cell-type proportion estimates based on type of biopsy**

- A. Violin plots of the cell-type proportion estimates across the needle (n = 434; dark blue) and surgical biopsies (n = 425; light blue). Boxplots within each violin plot show the median and interquartile range, and outliers are shown as dots.
- B. Zoomed in violin plots of the cell-type proportions from A with a different plot for each cell type. The y-axes differ across plots.

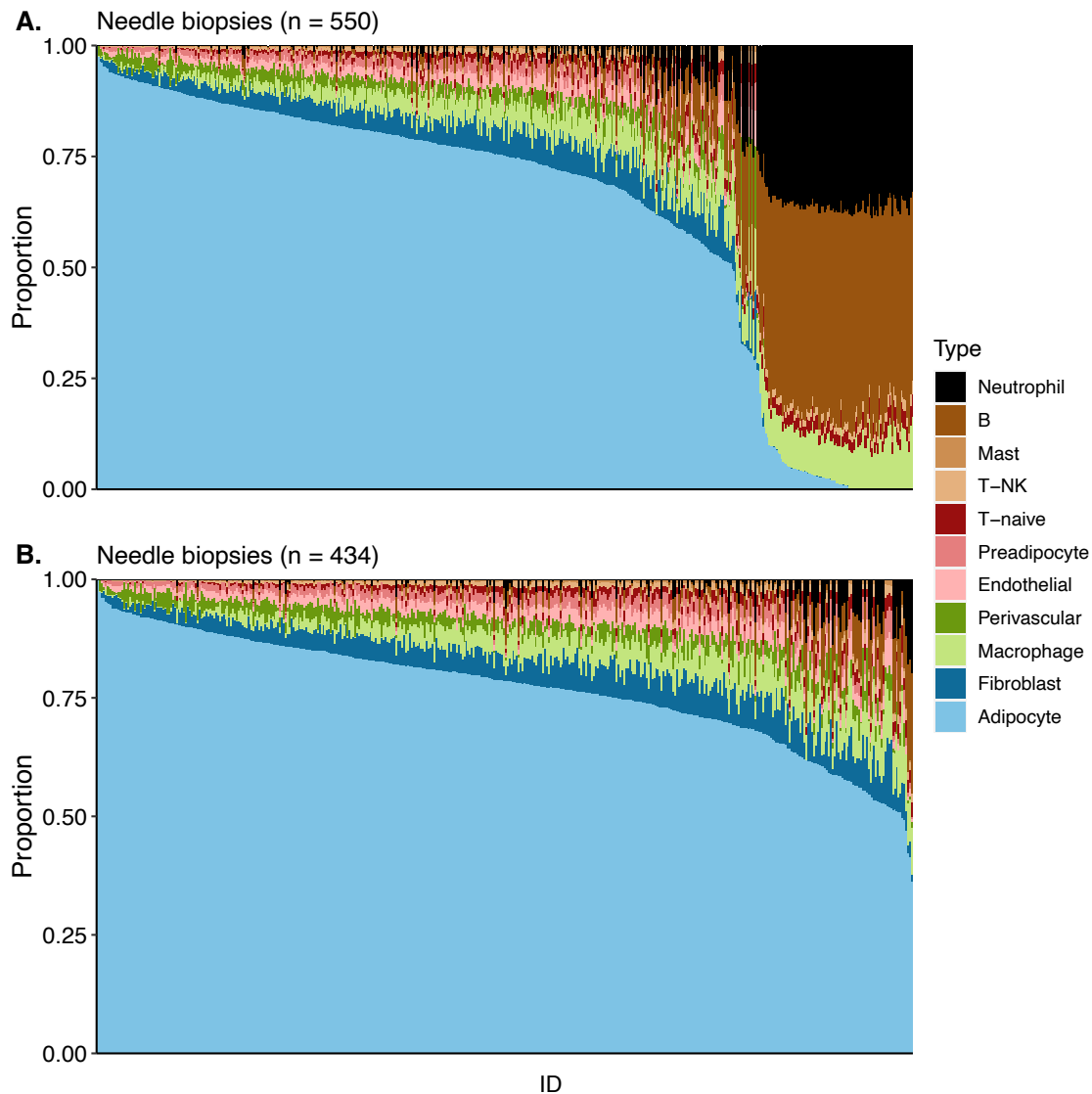
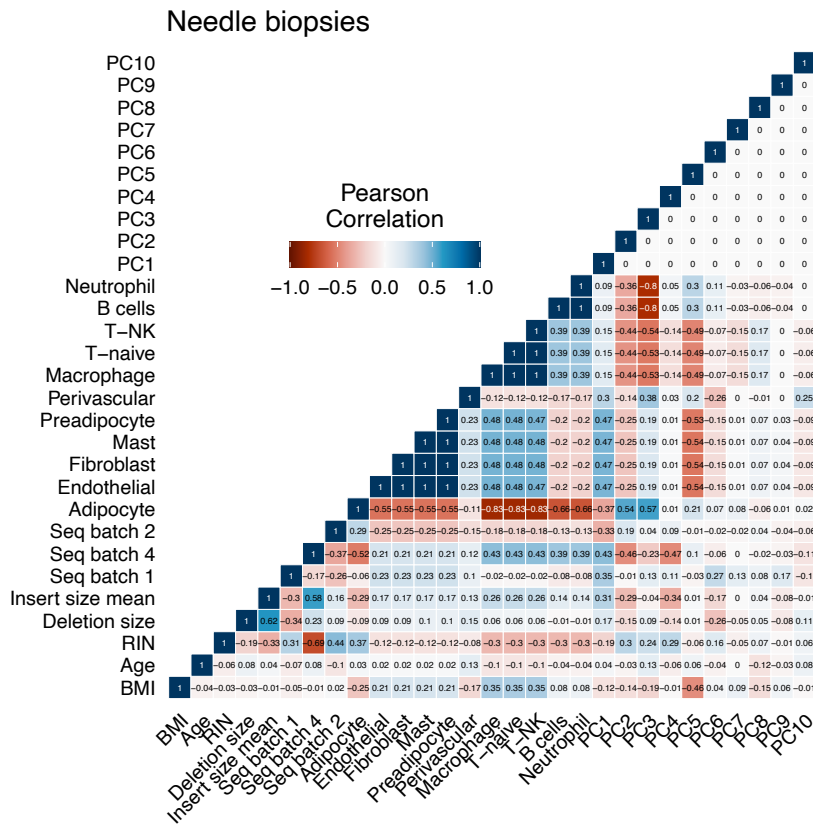


**Figure S7. Cell-type proportions across individuals for a larger set of needle biopsies (n = 550)**

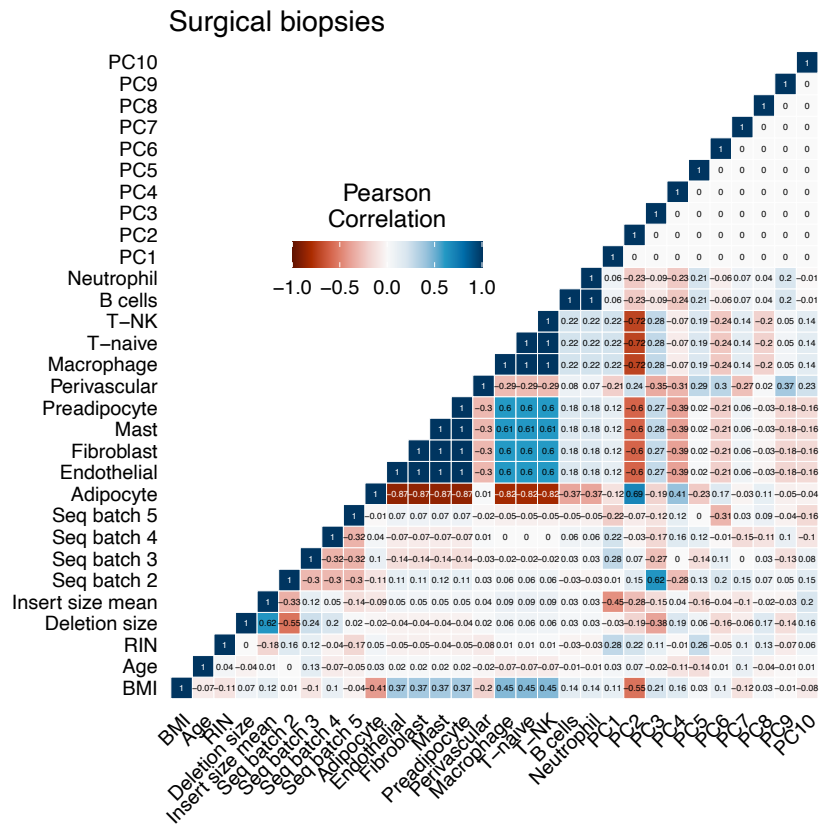
- Cell-type proportion estimates using the SCDC tree-based deconvolution method for each sample in 550 original needle biopsy samples, including the 434 samples used here. The other 116 samples had less than 50% adipose composition based on DESeq2 unmix deconvolution using subcutaneous adipose tissue from GTExv7 and Epstein Barr virus-transformed lymphocytes as a reference and were excluded (see Raulerson et al., 2019). Each sample is shown as a stacked bar representing the proportions of each cell type, colored as shown in the legend.
- Cell-type proportion estimates using the SCDC tree-based deconvolution method for each sample in 434 of the 550 needle biopsy samples in part A. The 116 excluded samples show large proportions of B cells and Neutrophils. Bars are slightly wider than in A.



A.



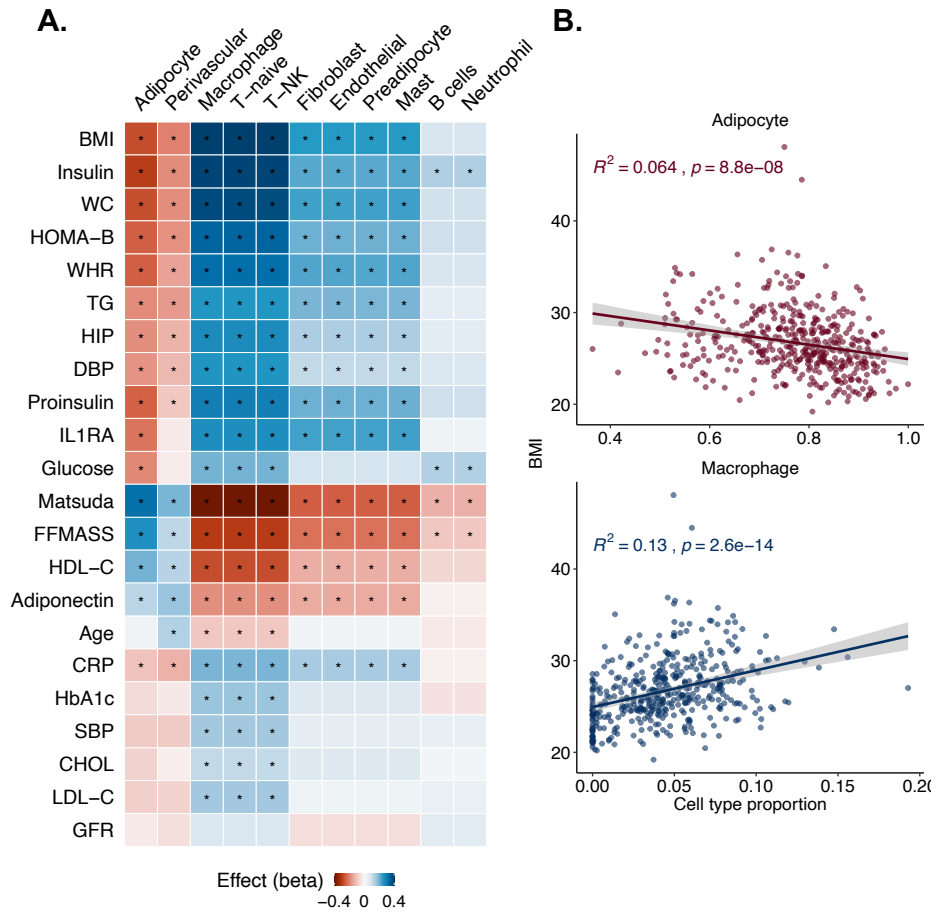
B.



**Figure S8. Correlations between technical covariates, cell-type proportions and gene expression PCs**

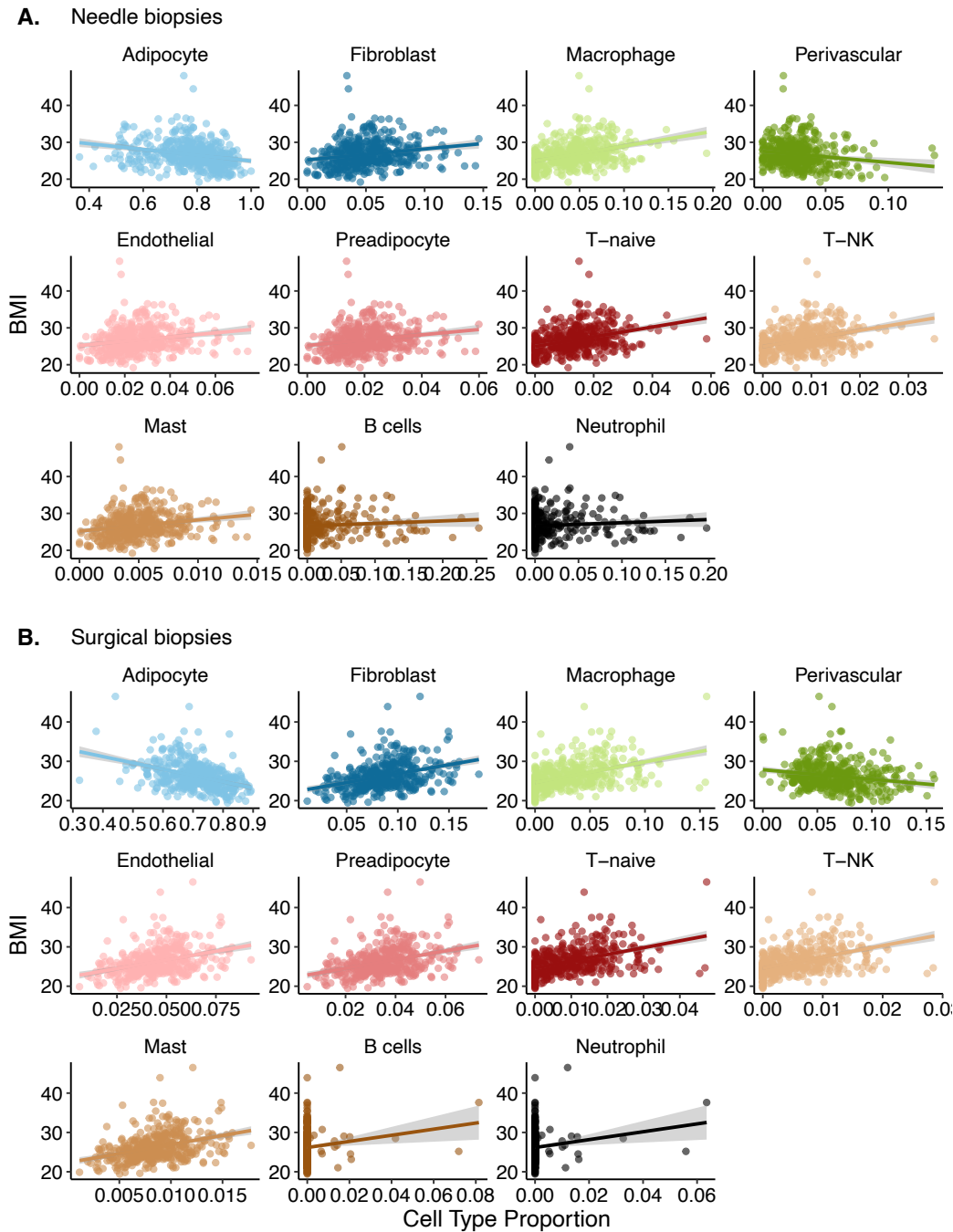
A. Heatmap of Pearson correlations between all technical covariates, cell-type proportions, and 10 gene expression principal components (PCs) for the needle biopsies (n = 434). Each box is a Pearson correlation value with the positive correlations in blue and the negative correlations in red. The intensity of the color increases with increasing Pearson correlation value.

B. Heatmap of Pearson correlations as in A for the surgical biopsies (n = 425).



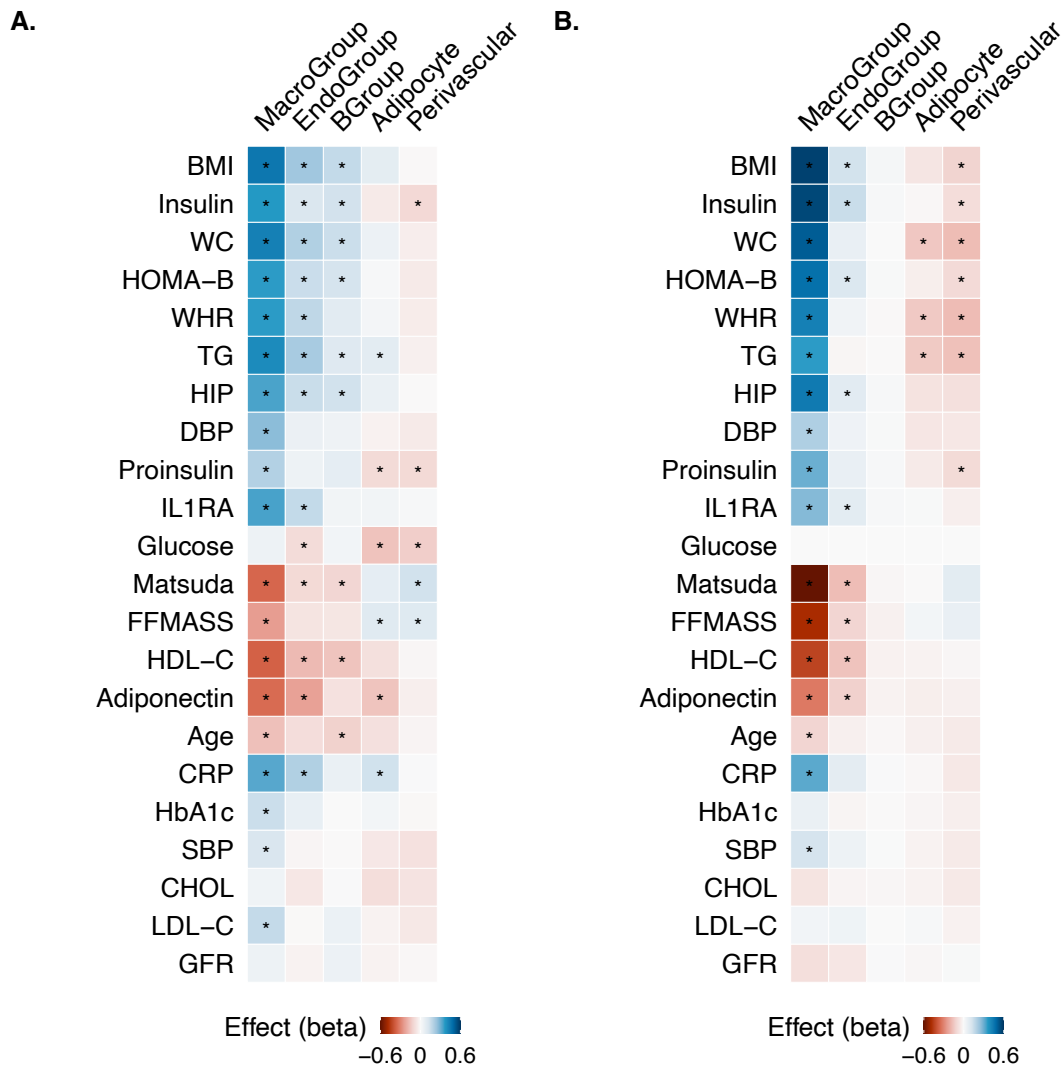
**Figure S9. Associations between cardiometabolic traits and cell type proportions for the needle biopsies**

- A. Heatmap of effect sizes for the association between inverse normalized cardiometabolic traits and scaled cell type proportions for the needle biopsies ( $n = 434$ ). Each box is a beta value shown in Table S7 with the positive effects in blue and the negative effects in red. The intensity of the color increases with increasing beta value. The boxes with an asterisk have a  $P$ -value  $\leq 0.05$ .
- B. Scatter plot of the association between BMI (y-axis) and cell type proportion (x-axis). Each dot is an individual sample ( $n = 434$ ). The top plot shows BMI versus adipocyte proportion, and the bottom plot shows BMI versus macrophage proportion. The linear regression lines are shown in solid color and confidence intervals (standard error) are shown in gray.



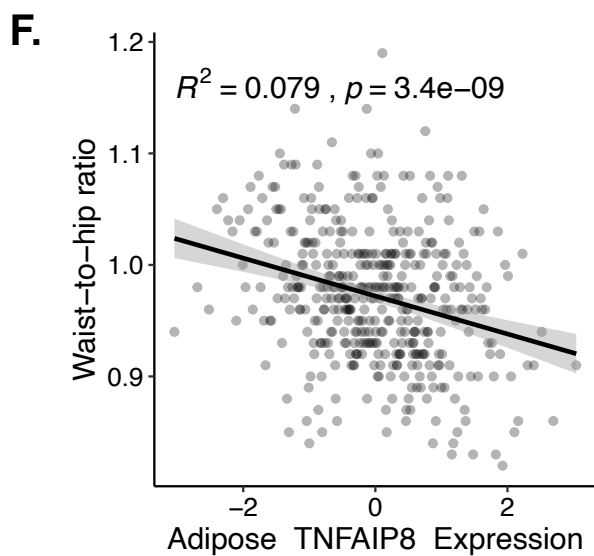
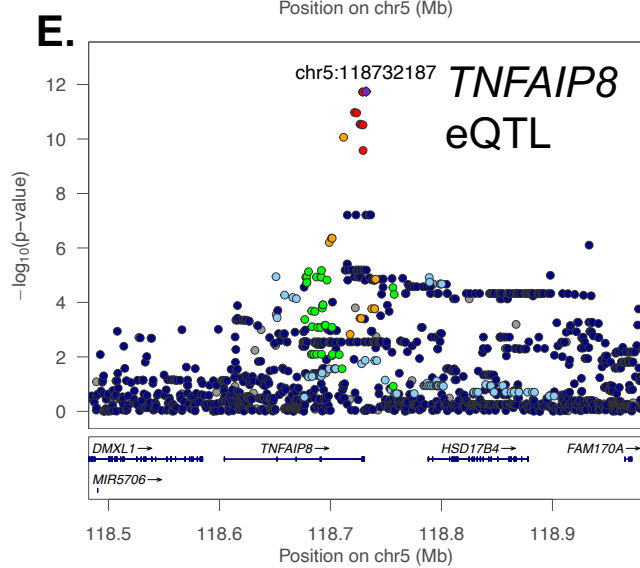
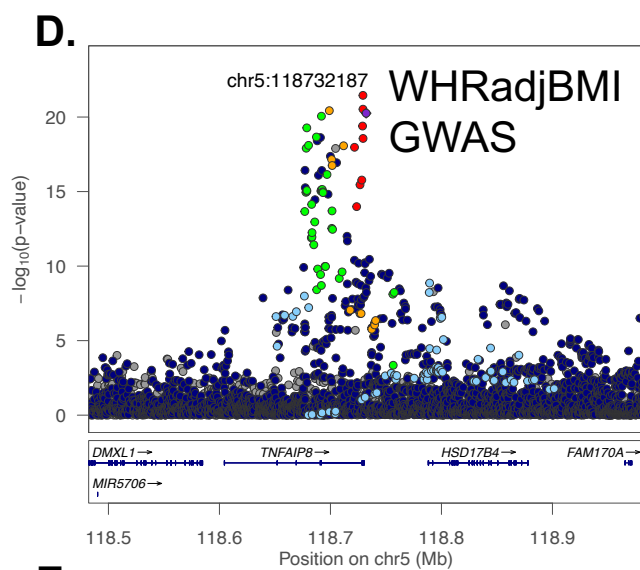
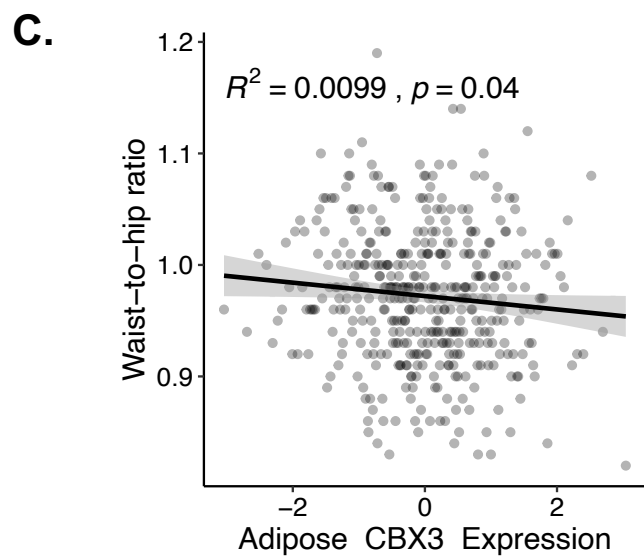
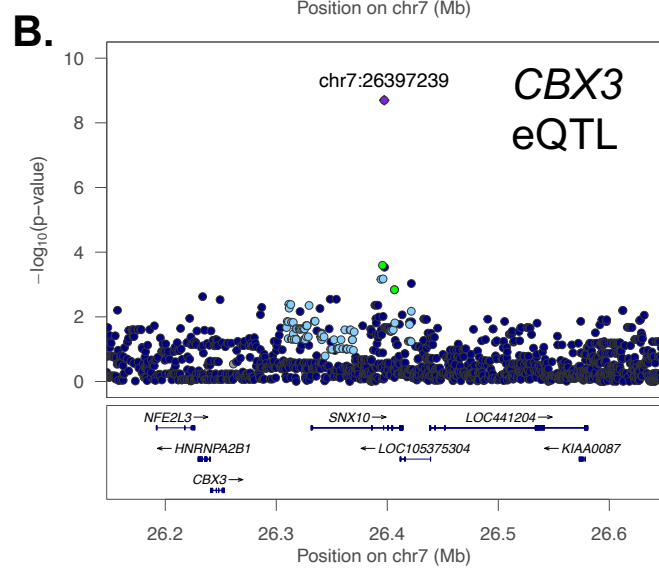
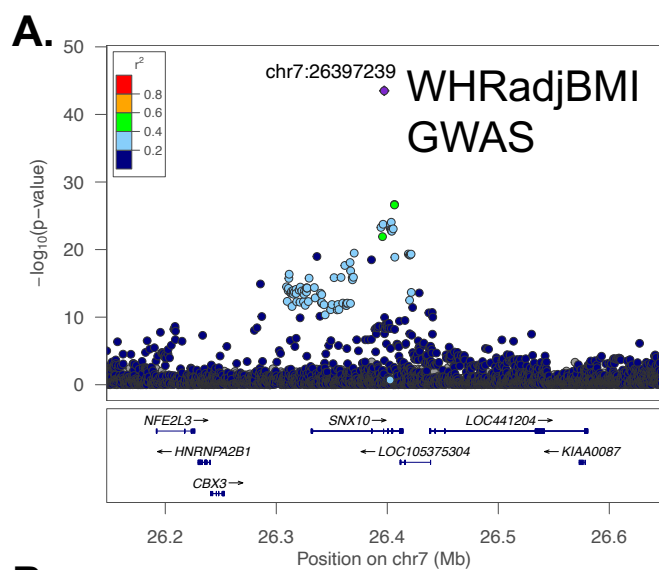
**Figure S10. Associations between cell-type proportions and BMI**

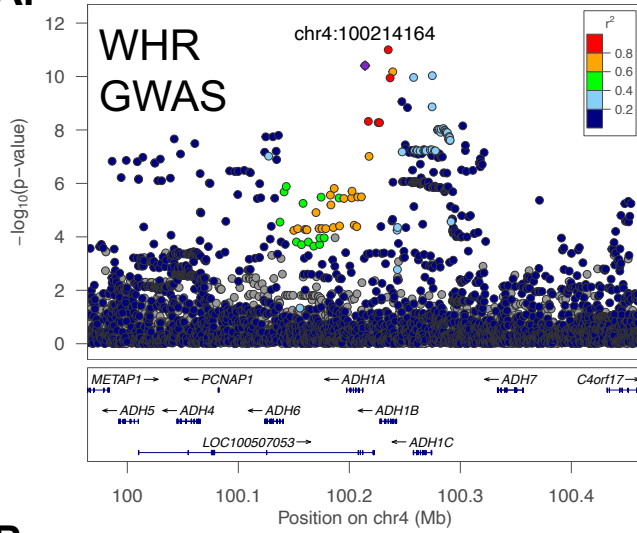
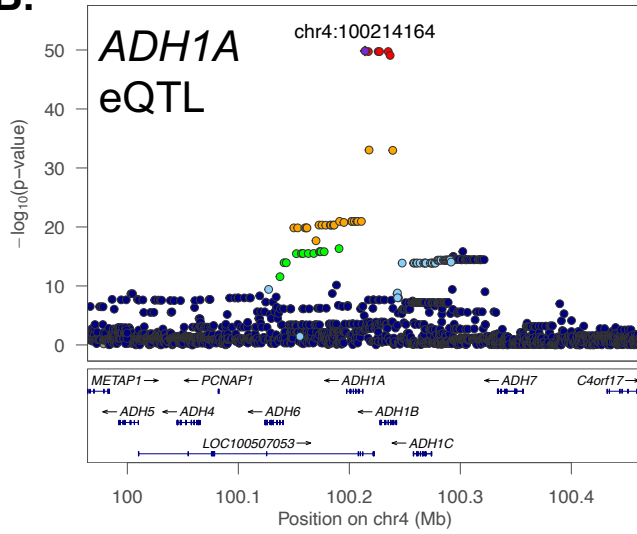
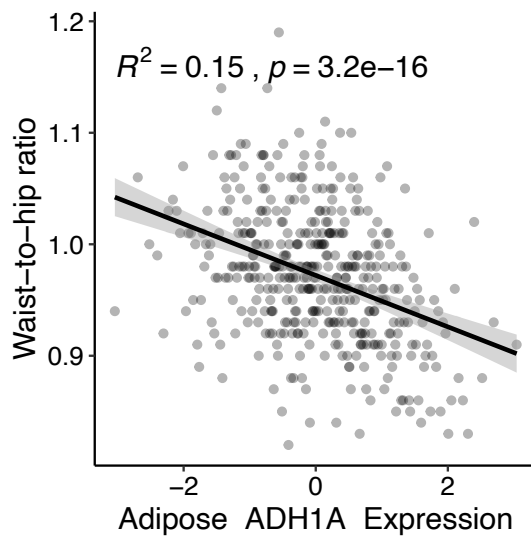
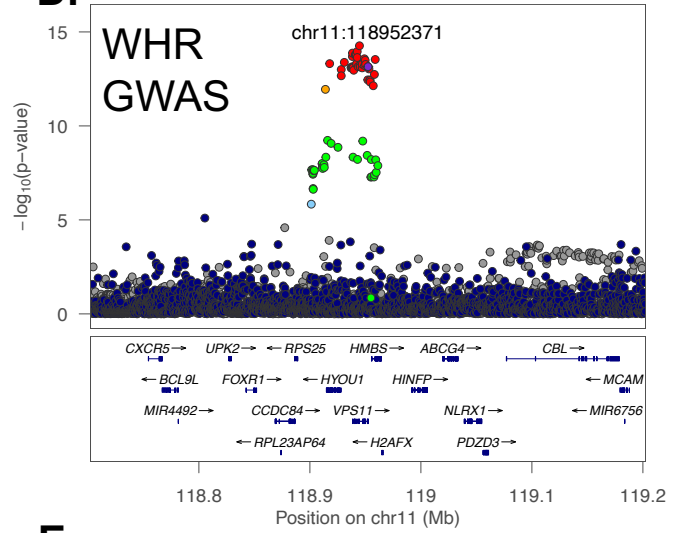
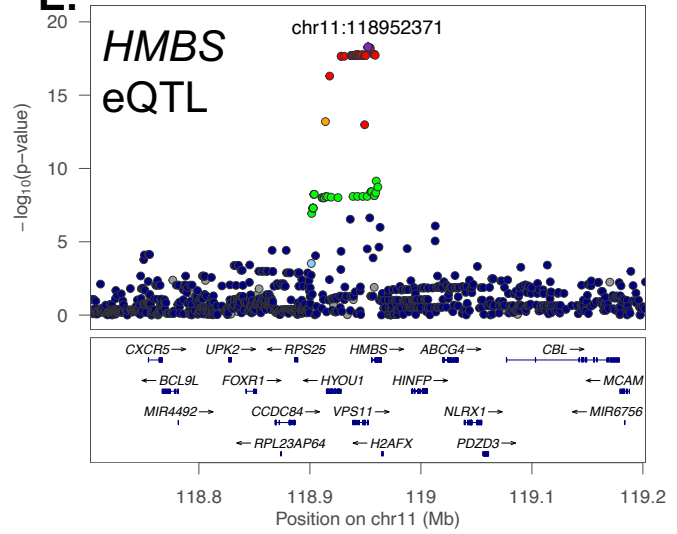
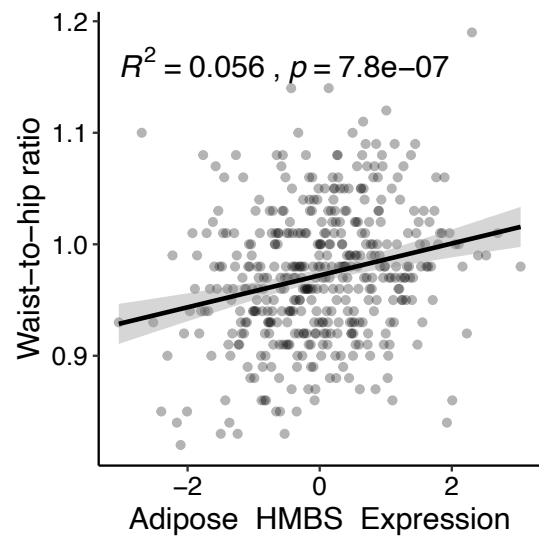
- A. Scatter plots of the associations between BMI (y-axis) and cell-type proportion (x-axis). Each dot represents an individual sample from the needle biopsies ( $n = 434$ ). Each plot is a different cell type and colored by cell type. The linear regression lines are shown in solid color and the confidence intervals (standard error) are shown in gray.
- B. Scatter plots of the association between BMI (y-axis) and cell-type proportion (x-axis) as in A for the surgical biopsies ( $n = 425$ ).



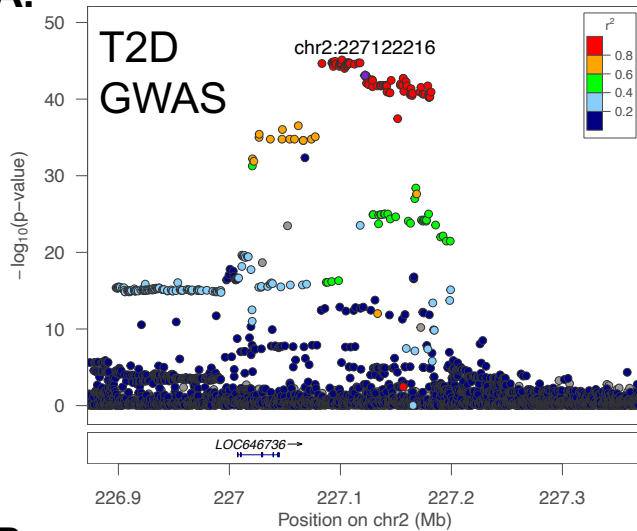
**Figure S11. Associations between cell-type proportions and cardiometabolic traits using a model to account for compositional data**

- A. Heatmap of effect sizes for the association between five cell-type proportion groups and inverse normalized cardiometabolic traits for the needle biopsies ( $n = 434$ ). The cell type groups were: MacroGroup (Macrophage, T-naïve, T-NK), EndoGroup (Endothelial, Fibroblast, Mast, and Preadipocyte), BGroup (B-cells, Neutrophils), Adipocyte, and Perivascular. Each box is a beta value shown in Table S7 with the positive effects in blue and the negative effects in red. The intensity of the color increases with increasing beta value. The boxes with an asterisk have a  $P$ -value  $\leq 0.05$ . All of the associations significant in both the Dirichlet regression and linear regression models showed the same direction of effect for surgical biopsies and 93% for needle biopsies.
- B. Heatmap of effect sizes for the association between five cell-type proportion groups and inverse normalized cardiometabolic traits as in A for the surgical biopsies ( $n = 425$ ).

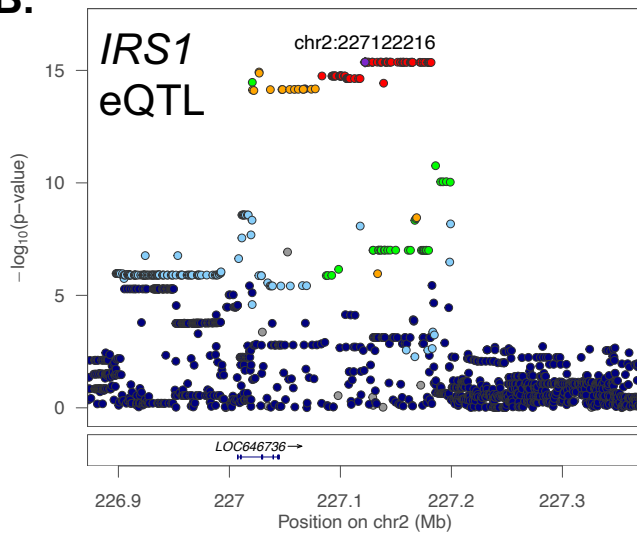


**A.****B.****C.****D.****E.****F.**

**A.**



**B.**



**C.**

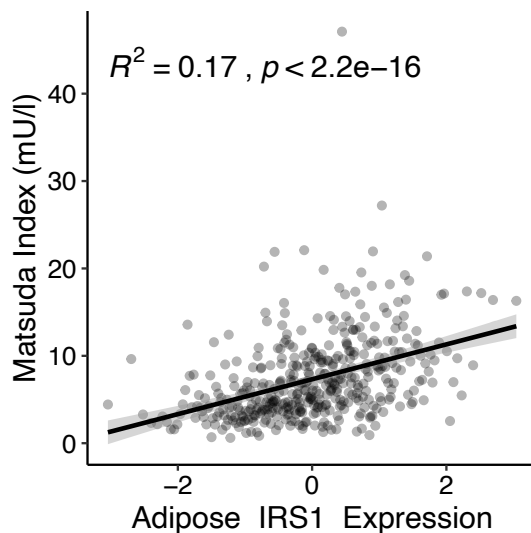


## Figure S12. Five GWAS-eQTL colocalizations supported by trait-gene association

- LocusZoom plots for WHRadjBMI, WHR, or T2D GWAS signal (WHR: Pulit et al 2019; T2D: Mahajan et al 2018) colocalized with an eQTL signal in adipose tissue (Raulerson et al 2019). The colors represent the pairwise linkage disequilibrium with the lead GWAS variant (purple diamond); red indicates high LD ( $r^2 > 0.8$ ) and blue indicates low LD ( $r^2 < 0.2$ ).
- LocusZoom plots for the eQTL signal in adipose tissue colocalized with the above GWAS signal.
- Scatter plot of inverse normal transformed gene expression and either WHR or Matsuda index (mU/l) in the surgical biopsy samples ( $n = 422$ ; 3 individuals without Matsuda index values were excluded). The linear regression line is shown in black and the standard error confidence interval is shown in gray.